Climate driven co-evolution of weathering profiles and hillslope topography generates dramatic differences in critical zone architecture

R. S. Anderson[1], H. Rajaram[2], and S. P. Anderson[3]

[1]INSTAAR and Dept. of Geological Sciences, University of Colorado Boulder, Boulder CO 80309.

[2]Dept. of Civil Environmental and Architectural Engineering, University of Colorado Boulder, Boulder CO 80309.

[3]INSTAAR and Dept. of Geography, University of Colorado Boulder, Boulder CO 80309.

Corresponding author: Robert S. Anderson (robert.s.anderson@colorado.edu)

Key Points:

• Distinctly different patterns of hillslope weathering can be attributed to differences in water recharge rate.

• Dry cases result in weathering that closely parallels the surface, while wet cases weather to the base of the groundwater flow system.

• Understanding the weathering patternrequires hydrologic models that include lateral groundwater flow, especially in the wet case.

Key Words:

Weathering, flowpaths, landscape evolution, hillslopes, climate

This article has been accepted for publication and undergone full peer review but has not been through the copyediting, typesetting, pagination and proofreading process which may lead to differences between this version and the Version of Record. Please cite this article as doi: 10.1002/hyp.13307

Abstract

Considerable debate revolves around the relative importance of rock type, tectonics, and climate in creating the architecture of the critical zone. We demonstrate the importance of climate, and in particular the rate of water recharge to the subsurface, using numerical models that incorporate hydrologic flowpaths, chemical weathering, and geomorphic rules for soil production and transport. We track alterations in both solid phase (plagioclase to clay) and water chemistry along hydrologic flowpaths that include lateral flow beneath the water table. To isolate the role of recharge, we simulate dry and wet cases and prescribe identical landscape evolution rules. The weathering patterns that develop differ dramatically beneath the resulting parabolic interfluves. In the dry case, incomplete weathering is shallow and surface-parallel, whereas in the wet case, intense weathering occurs to depths approximating the base of the bounding channels, well below the water table. Exploration of intermediate cases reveals that the weathering state of the subsurface is strongly governed by the ratio of the rate of advance of the weathering front, itself controlled by the water input rate, and the rate of erosion of the landscape. The system transitions between these end-member behaviors rather abruptly at a weathering front speed – erosion rateratio of ~1. While there are undoubtedly direct roles for tectonics and rock type in critical zone architecture, and yet more likely feedbacks between these and climate, we show here that differences in hillslope-scale weathering patterns can be strongly controlled by climate.

1 Introduction

The layer at the earth's surface in which water flows and weathers primary minerals to clays has been called the critical zone (CZ) for its importance to hosting terrestrial life on the planet (Anderson et al., 2007). The structure of this zone, including its vegetation, controlswater flow (Figure 1), and itself co-evolves with the topography over long timescales of order million years.

Chemical weathering within the critical zone plays key roles in geomorphology, biology and geologic hazards. Most directly, the degree of weathering can govern the susceptibility of rock to being entrained or released into the mobile regolith, and therefore serves as a regulator of soil formation. As the weathering architecture of the CZ influences the hydraulic conductivity of the subsurface, thereby controlling the flow rates and flow paths of water, it affects the chemistry of water that drains from hillslopes into rivers. CZ architecture is itself shaped by weathering and erosion processes largely driven by water. The thickness of the weathering zone also governs the depths from which plants may obtain nutrients. Finally, by affecting rock strength, the pattern of weathering may govern seismic shaking-induced landsliding (e.g., Gallen et al., 2015; Von Voigtlander et al., 2018).

The architecture of the subsurface has been illuminated with shallow geophysical methods (Befus et al., 2011; Clarke & Burbank, 2011; Leopold et al., 2013; Holbrook et al., 2014; Parsekian et al., 2015; Von Voigtlander et al., 2018), and by mineralogical and geophysical analysis of deep boreholes (Anderson et al., 2002; Banks et al., 2009; Buss et al., 2013; Rempe and Dietrich, 2018). These methods reveal different patterns and extents of weathering, from shallow to deep, from surface-parallel weathering to weathered layers that thicken upslope or downslope. The differences in critical zone architecture that these and other studies reveal have been attributed to causes ranging from climate to spatial variation in physical erosion rate to lithologic controls to tectonic processes.We propose and test a conceptual and numerical model focused on climate, specifically effective precipitation, to explain differences in weathering patterns.

The role of recharge rate on weathering front propagation and CZ evolution is well recognized, but has been explored largely based on one-dimensional models (White, 2002; Brantley & White, 2009; Maher et al., 2009). Multi-dimensional models have been developed only recently (Lebedeva& Brantley, 2013; Pandey&Rajaram, 2016; Brantley et al.,

2017; Braun et al., 2016). A complete model for weathering front propagation in a hillslope/interfluve should consider fluid flow and reactive transport in both the vadose zone (which is largely vertical) and the saturated groundwater system (where flow is largely horizontal/lateral, diverting the weathering front propagation). Especially at high recharge rates, as we discuss in this paper, unrealistic behavior results unless this lateral flow mechanism is properly represented. Another important element is the evolution of hillslope topography and the geometry of the water table, both of which are connected to changes in the channel at the base of the hillslope.

We develop a numerical model of a two-dimensional slice of an interfluve from drainage divide to channel that includes the weathering of rock, production of mobile regolith, transport of sediment, and transmission of water through the critical zone. Our modeling approach allows consistent exploration of the influence of recharge rate, subsurface hydrology (including lateral flow) on the evolution of CZ architecture. Our simulation results suggest that although a continuum of weathering patterns/CZ architectures is plausible, there are two key end-members, the transition between which occurs over a relatively small range of recharge rates. One end-member is development of a relatively thin, surface-parallel weathered zone, which occurs at low recharge rates. The other end-member, found at high recharge rates, is a weathered zone that extends well below the water table to the base of the groundwater system and produces deeply weathered interfluves.

2 Model for weathering and hillslope evolution

We develop a numerical model of evolution of a 2D cross section of a hillslope (Figure 1). Any such model must include rules for: 1) Entrainment of rock particles into the mobile regolith, commonly called the "soil production function" (for brevity, we use the terms soil and mobile regolith interchangeably). This process both lowers the rock-soil interface, and adds to the overlying soil thickness. 2) Transport of soil, the gradient in

transport contributing to the rate of soil thickening or thinning. 3) Incision of the channels that bound the interfluve and that therefore serve both as boundary conditions for the hillslope, and to transport soil and water out of the system. 4) Consistent representations of hydrology and reactive transport that conform to the boundary conditions imposed by other processes and hydroclimatic forcing.

We model essential elements of the hydrologic system within the evolving interfluve and the control of the hydrologic system on the chemical weathering. Soil production, sediment transport and channel incision together control topographic evolution. Within this evolving interfluve, we employ analytical solutions for the hydrologic flowfield and for the travel times of water through that field, which in turn allow tracking of the chemical evolution of the water as it reacts with the rock. This strategy necessitates simplifying assumptions, but this cost is compensated by model efficiency, and the ability to explore the major drivers of the chemical weathering patterns.

2.1 Geomorphic rules

The geomorphic components of the model follow closely those described in Anderson et al. (2013). Models of hillslope evolution require rules for the rate of lowering of the bedrock-mobile regolith interface (due to transformation or entrainment of particles from rock into soil)

$$\frac{\P z_m}{\P t} = -w \tag{1}$$

where z_m is the elevation of the bedrock-mobile regolith interface, t is time, and w is the rate of lowering of the interface. We also require an expression for the rate of change of the thickness of the mobile layer, H.

$$\frac{\partial H}{\partial t} = \left(\frac{r_r}{r_s} - 1\right) w - \frac{1}{r_s}\frac{\partial Q}{\partial x} \tag{2}$$

where ρ_r and ρ_s are the density of rock and the bulk density of soil, respectively, x is downslope distance, and Q is the mass flux of the mobile regolith. This conservation statement acknowledges a source term from release of rock into the soil from below, and the divergence of soil transport, Q, in the first and second terms, respectively. The elevation of the surface, z_s, is then calculated from the sum of the bedrock interface elevation and the soil thickness.

$$z_s = z_m + H \tag{3}$$

We therefore require model rules for the rate of detachment of rock into the soil (w), and for transport of mobile regolith downslope (Q). In addition, as the stream that bounds a hillslope serves as the boundary condition, we must specify the rate of incision of the stream.

2.1.1 Rate of bedrock lowering, *w*

The least well understood of the processes involved in the evolution of hillslopes is the lowering of the bedrock interface, or so-called soil production rate. In the present model we follow a common practice of assuming that the soil production rate is simply a function of the thickness of the soil (e.g., Heimsath et al., 1997; Anderson, 2002). Here we employ the simplest relation, in which the rate of soil production declines exponentially with soil thickness:

$$w = w_0 e^{-H/H_*} \tag{4}$$

where H_* is a soil depth at which the lowering rate of the rock interface has declined by a factor of e from that on bare rock, w_0.

2.1.2 Soil transport, *Q*

Once freed to move, soil is transported downslope in a manner that is governed by the local slope, the local regolith thickness, the climate, and material properties. The simplest rule for downslope transport of soil relates the soil mass transport rate, Q [M/LT], and local

slope, S: Q~-S. We advocate use of rules that require soil transport to vanish when soil thickness becomes negligible (e.g., Anderson, 2002). This is most easily captured in

$$Q = -k\rho_s H_{*q}\left[1 - e^{-H/H_{*q}}\right]S \tag{5}$$

where H_{*q} is a characteristic soil depth for the transport process, ρ_s is the bulk density of soil, and k has dimensions of a velocity (e.g., Johnstone&Hilley, 2015). A more process-specific rule for soil transport by frost creep is discussed in Section S1 of the Supplemental Materials; Figure S1 illustrates the differences among the rules.

2.2 Hydrology

In a wide range of settings, much of the weathering activity is believed to occur in the vadose zone, where fresh infiltrating recharge first encounters weathering minerals.In contrast to Braun et al.(2016), we consider water flow and reactive transport in both the vadose zone and below the water table. We envision steady state hydrology in a 2D hillslope subjected to a steady and spatially uniform recharge (or infiltration) rate U_0. The water table is assumed to be quasi-steady in time (it evolves slowly in response to lowering of the stream channel and topographic surface, but seasonality and hydrologic transients are not considered). For simplicity and an efficient analytical solution for the flowfield, we assign a uniform saturated hydraulic conductivity, K_{sat}. Future simulations will allow a spatially non-uniform saturated hydraulic conductivity field that evolves with weathering. In Section 2.2.1 below we discuss how we calculate the effective unsaturated hydraulic conductivity in the vadose zone.

We first calculate the expected water table geometry for the system, $z_w(x)$. On a hillslope of length L, with a bounding channel of elevation z_b and water depth h_c, the water table geometry obtained from the standard Dupuit approximation is (Figures 1 and 2):

$$z_w = z_b + \sqrt{h_c^2 + \frac{U_o}{K_{sat}}\left(L^2 - x^2\right)} \tag{6}$$

Within the vadose zone between the ground surface and this water table, the flow of water is assumed to be vertical and based on the widely used unit gradient approximation (i.e. purely gravity driven flow). Groundwater flowpaths must segue between these vertical paths and the horizontal flow at the exit to the channel. Importantly for calculation of chemical reactions along these flowpaths, this analytical solution also allows calculation of travel times along these paths. Based on using the two-dimensional continuity equation to derive the vertical flux component, Strack (1984) showed that the streamlines for the steady state flow field in a hydraulically homogeneous medium are hyperbolic (Figure 2):

$$z(x;x_i) = z_b + \left[z_w(x_i) - z_b\right]\frac{x_i}{x};x > x_i \tag{7}$$

where x_i is the initial horizontal location of the streamline where it crosses the water table, $z_w(x_i)$ is the elevation of the water table at that location, and $z(x;x_i)$ is the elevation at location x of the streamline that crossed the water table at location x_i. The advective travel time of the water (the time, T_v, from infiltration at the surface of the hillslope, z_s, to any position along itsflowpath) is controlled by the advective solute velocity (U_o/θ) for a given water content θ in the vadose zone (the calculation of θ for unit-gradient flow is further discussed below in Section 2.2.1), and linearly increases with depth within the vadose zone:

$$T_v(x;x_i) = \frac{(z_s(x_i) - z)}{U_0 / q};z > z_w(x_i) \tag{8}$$

Subsequently, the additional travel time within the groundwater system increases roughly logarithmically with horizontal distance traveled when the water table has relatively low relief (Gelhar& Wilson, 1974; Chesnaux et al., 2005):

$$T_{gw}(x;x_i) = \frac{h_c \phi}{U_0}\ln\left(\frac{x}{x_i}\right);x > x_i \tag{9}$$

where ϕ is the effective porosity. It is readily evident from equations (8) and (9) that the recharge rate exerts a strong influence on the travel time structure within the hydrologic

system. A more general expression for the travel time within the groundwater system is presented by Chesnaux et al. (2005).

2.2.1 Porous medium properties and vadose zone flow

The hydrologic framework for our model is based on a hillslope with a length of L = 100 m, and a stream water depth h_c = 3 m (see Figure 1). We use values of saturated hydraulic conductivity K_{sat} = 0.05 m/day and porosity ϕ of 0.1, for unweathered fractured granitic rocks (Freeze & Cherry, 1979). With the above value of K_{sat}, the elevation of the water table is calculated from equation (6). In the vadose zone above the water table, the water content θ is calculated by assuming unit gradient conditions with the specified recharge:

$$U_0 = K_{unsat}(q) = K_{sat} k_r(q) \tag{10}$$

Here θ, K_{unsat}, and k_r refer to the water content in the vadose zone, unsaturated hydraulic conductivity and relative permeability, respectively. The assumption of unit-gradient conditions is no doubt a simplification, but is justified considering other higher-level simplifications invoked, such as the assumptions of steady-state climatic forcing and recharge. These simplifications allow us to address differences in the coupled behavior of hydrology, weathering and geomorphology in the wet versus dry cases, without introducing too much complexity. Equation (10) requires a relationship between water content and relative permeability, $k_r(\theta)$, for which we use the Brooks-Corey model (Brooks & Corey, 1964):

$$k_r(q) = \left(\frac{q - q_r}{f - q_r} \right)^{3+2/\lambda} \tag{11}$$

where λ is the pore-size distribution index and θ_r is the residual saturation. We assume a value of 0.1 for λ, which is consistent with fine-grained materials representing the rock matrix, and a value of 0.02 for θ_r. Although fractured rock behaves like a dual continuum in which wide fractures drain at relatively low suction, they occupy a relatively small volume fraction, and

the suction-saturation curve is likely dominated by the properties of the rock matrix at low recharge rates. In the wet and dry cases, respectively, the recharge rates are 0.12 m/yr ($3.3\text{x}10^{-4}$ m/day) and 0.02 m/yr ($5.5\text{x}10^{-5}$ m/day). We emphasize that this is the recharge rate to the deep flow system, and reflects both precipitation and evapotranspiration; the rates we have chosen are representative of eastern US and mountain West recharge rates (Döll and Fielder, 2008). From these recharge rates we calculate the corresponding water contents θ in the vadose zone of 0.084 and 0.08, respectively. These water contents are not significantly different because the recharge rates in both cases are much smaller than the saturated hydraulic conductivity. However, the travel time through the vadose zone is expected to be much shorter in the wet case, as evident from (8), but also because the water table is shallower (see (6)).

2.3 Chemical weathering

We now explore the consequences of the travel time (T_{gw}) structure within the interfluve (Figure 3) on the chemical weathering field. While many minerals within a rock will weather at different rates, we choose to treat the system as having one mineral that is most susceptible to weathering. Models based on monomineralic systems have been used extensively to derive insights on weathering (e.g., Maher, 2010; Brantley &Lebedeva, 2011; Lebedeva et al., 2010; Lebedeva& Brantley, 2013). To this end, we track the weathering of plagioclase feldspar along hydrologic flowpaths within the 2D hillslope. The rate of chemical weathering of the primary mineral is captured by:

$$\frac{\partial P}{\partial t} = -k_P\left(C_{eq} - C\right)\frac{P}{P_0} \tag{12}$$

where P is the molar mineral concentration of the primary mineral (here plagioclase) in the rock [moles/m^3], P_o is its concentration in fresh rock, k_P is the reaction rate constant [1/T], and C is the concentration of the dissolved primary mineral in the fluid [moles/m^3]. Two

factors govern the reaction rate: the fraction of the concentration of plagioclase remaining in the rock, here represented by(P/P_o), and the approach of the concentration of dissolved mineral in the fluid to the equilibrium concentration, C_{eq}.

The reactive transport equation for the concentration of dissolved mineral in the infiltrating water may be conveniently written along flow lines (streamlines), as:

$$\frac{\partial C}{\partial t} + V_s \frac{\partial C}{\partial s} = k_P \left(C_{eq} - C \right) \frac{P}{P_0} \tag{13}$$

where s is a curvilinear coordinate along a streamline and V_s denotes the (spatially variable) velocity component along streamlines. Streamline-based models have been developed previously for reactive transport modeling in other contexts over the last two decades (e.g., Crane & Blunt, 1999; Simmons et al., 1995). Note that equation (13) assumes advection-dominated transport and neglects diffusion-dispersion terms. This approximation has been adopted in previous reactive transport models for weathering and captures the behavior quite well in porous media under most conditions. However, this approximation may not be valid in fractured rock where matrix diffusion plays a significant role in controlling weathering front propagation (e.g., Pandey and Rajaram, 2016; Rajaram and Arshadi, 2016), or under diffusion-dominated conditions (e.g., Lebedeva et al. 2007). Following Gelhar and Collins (1971) and Dagan and Cvetkovic(1996), equation (13) can be rewritten by transforming to advective travel-time coordinates as defined as:

$$T(s) = \int_0^s \frac{ds'}{V_s(s')} \tag{14}$$

where $T(s)$ denoted the travel time to coordinate s and s' is a dummy variable for integration. Assuming quasi-steady state behavior for dissolved mineral transport, justified by the large ratio of P_o to C_{eq} (Ortoleva et al., 1987), the transient term in the resulting transformed equation may be dropped, yielding for the rate of change of concentration of dissolved species in the fluid:

$$\frac{\P C}{\P T} = k_P(C_{eq} - C)\frac{P}{P_0} \quad (15)$$

where T denotes the travel time along a streamline, defined by equations (8) and (9). In the simulations presented herein, we have employed P_o=3x10^3 moles/m^3, C_{eq}=0.2 mole/m^3, and k_P=8.4x10^{-9} s^{-1} (e.g., Brantley &Lebedeva, 2013).

2.4 Numerical implementation

The algorithms we have described are embedded in a finite difference numerical model. We prescribe initial conditions of topography, soil thickness, and rock properties that include density, porosity, hydraulic conductivity, and reactive mineral concentration. As the topography is symmetrical, we report only one half, between the divide and one channel. We prescribe the lowering of the channel at the edge of the hillslope at a rate e as a boundary condition. As the base of the channel, z_b, governs the base of the groundwater flowfield, lowering of the channel brings fresh rock into the weathering system. Water infiltrates at a steady rate U_o, with initial dissolved mineral concentration C_o (taken to be zero). Water flow line (streamline) trajectories are vertically downward in the vadose zone, and calculated from equation (7) below the water table. Travel times are calculated from equation (8) in the vadose zone and equation (9) below the water table. The dissolved mineral concentration field along each flow line is calculated from equation (15) and the mineral reaction rates are calculated from the right hand side of equation (15). The mineral reaction rate field is interpolated from the flow lines onto a fixed rectangular grid and equation (12) is used to update plagioclase concentrations. The updated plagioclase concentrations are used while solving the quasi-steady state transport equation (15) in the subsequent time-step. The bedrock – soil interface is lowered at a rate governed by the local soil thickness using equation (4). The soil discharge rule, equation (5), is implemented using a staggered grid, and the thickness of soil is updated using the mobile regolith conservation equation (2). The

surface elevation $z_s(x_i)$ is updated in each time step, and serves as the upper boundary for the water flow and reactive transport calculations.

3 Numerical Model Results

3.1 Comparison of dry vs wet end-member cases

To illuminate weathering fields in different climates, we first run the model with two end-member climate forcings. In both cases the initial conditions, rock properties, and efficiency of both soil transport and bedrock weathering are held constant. Only the rate of water delivery (set by the recharge rate U_0) to the landscape differs, fixed at 0.02 m/yr in the dry case and 0.12 m/yr in the wet case. This sets both the water table geometry and the flow velocities through the subsurface. All other hydrologic properties are held uniform and steady as discussed in section 2.2.1. The bounding channel incision rate, e, is held steady at 30 m/Myr. We run each model for 1 million years, roughly the time required for steady state topography to evolve ($T_t = R/e$, where R is the steady state relief, and e is the erosion rate of the bounding channels). The topography, the soil thickness, and the weathering fields have all achieved a steady state in the moving frame of reference tied to the local channels.

The linear increase in water travel times with depth in the vadose zone imposed by equation (8) sets the time for water to reach the water table (Figure 2). Travel times continue to increase as described by equation (9) along the hyperbolic trajectories in the groundwater toward the exit at the channel. Longer trajectories of water parcels initiated near the ridge have considerably greater total travel times upon exit. The travel times of water along trajectories are significantly longer in the dry case than the wet case, reflecting the 6-fold difference in recharge rate. Although the streamline patterns shown in Figure 2 were derived based on a highly simplified hydrologic framework that assumes unit gradient conditions in the vadose zone and the Dupuit approximation for the water table, it is interesting to note that the behavior closely resembles that obtained with more sophisticated analytical solutions for

unsaturated-saturated flow (e.g., Ameli et al. 2016). However, our assumption that the base of the groundwater flow system is flat and coincident with the stream channel bed does not capture the deeper groundwater flow structure.

The pattern of weathering differs significantly between the dry and wet cases as the topography evolves (Figure 3). In the dry case, plagioclase remains throughout the interfluve; plagioclase loss is restricted to a thin surface-parallel zone of order 1-2 m thickness, with the exception of a region ~ 10 m wide near the channel. In contrast, in the wet case, transformation of plagioclase to clay is nearly complete within the entire interfluve, with the exception of a few-meter thick zone at the base of the groundwater flow system.At 1000 kyr in the dry case, the reaction extent profile has become steady with time in the reference frame of the moving topography; it is highest at the surface and vanishes within 5 meters. In the wet case, plagioclase is completely transformed, leaving a boundary layer at the base of the groundwater system in which reaction extent decreases smoothly to zero. This stark difference in behavior reflects the fact that in the dry case the rate of lowering of the channel outpaces the rate of propagation of the weathering front, whereas in the wet case the weathering front outpaces the channel incision.

Evolution of the weathering fields (Figure 3) may be interpreted by inspecting the evolving weathering rate fields (Figure 4). In the dry case, the rate field rapidly evolves to a pattern in which significant weathering rates are always confined to the near-surface soil and rock. Given the low recharge rates, water travels slowly downward in the vadose zone, increasing in solute concentration, and thereby decreasing in reaction rate (Equation 15).

In the wet case, rates of transformation of plagioclase to clay are more complex, as they reflect the passage of a weathering front through the hillslope and are influenced by increasing plagioclase depletion near the surface. Rates are very high at the outset, limited only by the rate constant and equilibrium concentration ($k_p C_{eq}$ in Equation 15). By 50 kyr,

maximum reaction rates have declined but remain relatively high near the topographic surface, extending at significant rates to ~ 10 m depths. Rates remain low in the core of the interfluve. By 250 kyr, the intensity of weathering has declined near the surface, with the exception of a high intensity spot near the toe of the slope, and is moderate to high in the core of the interfluve. A weathering front has propagated along flow lines, leaving the near-surface depleted in plagioclase; rates are high only where significant plagioclase remains (low reaction extent in Figure 3). By 1000 kyr, the weathering rate field is steady; weathering rates are low in the entire interfluve with the exception of a several-meter thick region near the base of the groundwater system. The pattern reflects the complete transformation of plagioclase to clay in this wet environment on timescales over which the topography reaches a steady parabolic form.

3.2 Sensitivity of 2D model results to choice of porosity, water content, and medium alteration

We acknowledge that the model and end-member cases presented are simplified. They do not consider spatial variations in permeability, or the alteration of porosity and permeability either due to weathering or due to a host of other near-surface processes (tree roots, frost cracking, expansion and contraction due to thermal and wetting cycles, and animal burrowing). Soil is transported by diffusive processes, excluding for example, transport by landsliding. Here we present a sensitivity analysis that explores at least some of such feedbacks. In general, a fully coupled model incorporating two-way feedbacks between weathering, evolving porous medium properties (porosity, permeability, unsaturated flow constitutive parameters) and hydrology, is expected to provide a more complete description of the long-term evolution of the hillslope. However, the semi-analytical simplicity of the modeling approach employed in the main body of the manuscript will no longer hold and a full numerical treatment of unsaturated-saturated flow in a heterogeneous medium would be

required. In recent work that employed such a numerical treatment (Pandey&Rajaram, 2016), we found that in the case of prescribed flux boundary conditions, the influence of porosity and permeability feedbacks is not strong, largely because (prescribed) hydrologic fluxes are not significantly altered by these feedbacks. To illustrate this behavior, our sensitivity analysis is based on running the simulations shown above again, but with the properties of the medium altered from weathering. We use two approaches, one based on field observations of weathered granite and one based on a commonly used empirical porosity-permeability relationship, to generate three different cases.

An end-member of hydraulic properties in weathered rock based on field measurements comes from Katsura et al. (2006), who document a high hydraulic conductivity and unusually high porosity in weathered granite, with K_{sat} = 0.8 m/d, a porosity of 0.25-0.4 and commensurately high saturated water content θ=0.28. In fact,Katsura et al. (2006) compare their measurements to other field measurements in weathered granite that indicate a porosity closer to the 0.1 value we assumed in the base case simulations shown in Section 3.1. In Figure 5a, we present model results using K_{sat} = 0.8 m/d, porosity ϕ=0.35, and water content θ=0.28. With these assumed values, the degree of saturation θ/ϕ is consistent with the value assumed in the base case in Section 3.1. The high hydraulic conductivity yields a much flatter water table (Fig. 5a). The high water content slows the advective water velocity, allowing more accumulation of solutes, and lowers the rate of weathering front propagation. This results in a transitional state in which the weathering is relatively thin (although much thicker than in the dry base case) and surface parallel near the divide, but becomes much deeper near the base of the hillslope. This transitional case is therefore something of a hybrid between dry and wet case.

Quantitative understanding of the alteration of porous medium structure due to weathering, especially under partially water-saturated conditions is limited. We expect that

not only the porosity and saturated permeability, but also the suction-saturation curve and relative permeability function will evolve with weathering. However, there is very little observational basis for quantifying changes in parameters involved in the suction-saturation and relative permeability relationships due to weathering. For the purposes of a sensitivity analysis, we employ the commonly used Kozeny-Carman porosity-permeability relationship (Freeze and Cherry, 1979), which has admittedly not been extensively tested experimentally, as a valid representation of permeability change due to weathering. We assume for simplicity that the pore-size distribution index is not altered by weathering.

To calculate the expected changes in the hydrologic properties of the medium due to weathering, we evaluate porosity generation by isovolumetric weathering. We assume that albite (bulk density = 2620 kg/m^3 and molecular weight = 263 g) weathers to secondary kaolinite (bulk density = 2600 kg/m^3 and molecular weight = 258 g). The stoichiometry of the weathering reaction dictates that 1 mole of albite produces 0.5 moles of kaolinite. For an initial volume fraction of albite in the solids (V_{po}) of 0.3, and complete isovolumetric weathering of albite to kaolinite, the porosity change due to weathering can be calculated from (note that $\phi_{old} = 0.1$):

$$\phi_{new} = 1 - (1 - \phi_{old})\left[\left(1 - V_{po}\right) + 0.5 V_{po} \frac{258}{263}\frac{2620}{2600}\right] = 0.24 \quad (16)$$

The corresponding change in hydraulic conductivity is calculated from the Kozeny-Carman relationship as:

$$K_{sat,new} = \frac{\phi_{new}^3}{\phi_{old}^3}\frac{\left(1 - \phi_{old}^2\right)}{\left(1 - \phi_{new}^2\right)} K_{sat,old} = 0.97 m/day \quad (17)$$

Based on these new parameters, assuming that residual saturation in Equation 11 remains the same fraction of porosity and that the pore size distribution index remains the same, the water content θ_{new} in the vadose zone for the altered medium is calculated as 0.18 in the wet case

and 0.17 in the dry case, respectively. An alternative viewpoint on the evolution of K_{sat} is that if the overall saturated hydraulic conductivity is dominated by fractures, then isovolumetric weathering of matrix blocks will produce no change in fracture apertures (White et al. 2001; Pandey and Rajaram, 2016), and hence no change in the overall saturated hydraulic conductivity. It is also interesting to note that Katsura et al. (2006) found no apparent relationship between ϕ and K_{sat} for a few different weathered granite sites, with actual K_{sat} values ranging from about 0.08 to 0.8 m/day. Based on the above considerations, we consider two other end members: the second sensitivity analysis simulation in Figure 5b shows the effect of using ϕ_{new} and θ_{new}, but leaving K_{sat} unchanged, while Figure 5c shows the effect of altering all three properties. The altered K_{sat} from equation (17) above is in fact higher than the field measurement reported by Katsura et al. (2006) at their study site.

We find that the pattern of weathering is indeed dominated by the recharge rate. By comparing the wet base case in Figure 3f and the cases in Figures 5b and 5c, one can see that the essence of the wet case -- i.e. that feldspars are deeply weathered -- is retained over a reasonably wide range of hydraulic properties (K_{sat} and ϕ and θ) meant to bracket unweathered and deeply weathered cases. The conductivity, K_{sat}, largely controls the geometry of the water table. The high conductivity in the cases shown in Figures 5a and 5c results in a low-relief water table. But the similarity of the weathered profiles in Figures 5b and 5c, despite a factor of 20 difference in K_{sat}, suggests that the weathered profile is largely controlled by the input of water from recharge prescribed at the surface, and hence climate, rather than hydraulic properties. Comparing the profile of the wet case in Figure 3f with that in Figure 5b suggests that the weathering profile behavior is slightly sensitive to ϕ and θ. The much higher porosity and water content in the case presented in Figure 5areduces the advective solute velocity and results in a profile that is in-between the wet and dry base cases (Figure 3c,f). Dry cases (not shown here) in which similar ranges of hydraulic properties

were explored show little to no change: the weathering pattern remains surface-parallel and thin, as in Figure 3c.

3.3 Sensitivity of 2D model results to recharge: intermediate cases

Here we explore the sensitivity of the steady state weathering patterns within the interfluve to the choice of water recharge rate U_0. While our exploration is not meant to be exhaustive, we ran several cases of water delivery that are intermediate between our dry (U_0 = 0.02 m/yr) and wet (U_0 = 0.12 m/yr) cases, while keeping the hydraulic properties the same for all cases. We find that the transition from thin surface-parallel weathering pattern to deep weathering occurs over a relatively narrow range of recharge (Fig. 6). As the recharge rate increases from the dry end-member value, the weathering front gets deeper while retaining an essentially 1D character. Further increases in recharge rate lead to penetration of the weathering front below the water table near the stream, while retaining the 1D character upslope (closer to the ridge) where the water table is deeper. As the recharge rate is increased even further, the location of the transition between the 2D and 1D behaviors progressively moves upslope because the travel times through the vadose zone become short enough for weathering to penetrate below the water table, eventually leading to nearly complete weathering as in the wet end-member. We chose the recharge rates considered in Figure 6 specifically to highlight patterns that were something of a hybrid between the 1D and 2D behaviors. When recharge is increased further, to 0.05 m/yr (not shown), the pattern is virtually indistinguishable from the wet base case: weathering throughout the interfluve penetrates to the base of the groundwater flow system. Wet-looking profiles can indeed arise in relatively dry conditions. For recharge rates lower than 0.03 m/yr, the pattern is similar to the dry base case, but the depth of the weathering front declines as the recharge rate is reduced.

3.4 1D exploration of rate of weathering front propagation

Our 2D models illustrate that the velocity of the weathering front, identified by the sharp gradient in reaction extent, is much lower in the dry case than in the wet case (Figure 3). It is the ratio of the weathering front velocity, w_f, to the erosion (or exhumation) rate e that serves as a key control on the development of the weathering profile. We further illuminate this point with a 1D model that allows us to focus on controls on weathering front propagation into fresh rock over time.

In a 1D stationary column of rock subjected to a steady supply of water at the top of the column at the recharge rate of U_o and water content θ, with reactive transport described by equation (15), the weathering front velocity is given by:

$$w_f = \frac{U_0 / q}{\left(1 + \frac{P_0}{C_{eq}}\right)} \approx \frac{U_0}{q}\left(\frac{C_{eq}}{P_0}\right) \tag{18}$$

Here the solute velocity in equation (13) is represented as U_0/θ, a constant in this one-dimensional system. The water content θ is equivalent to the effective porosity for saturated flow conditions. The weathering front speed is scaled by the solute velocity U_0/θ, modulated by a very small factor (in parentheses) that reflects the ratio of the saturated concentration of reactants in the fluid to the mineral concentration of the solid phase. For example, in the wet case, U_0=0.12 m/yr, $P_o = 3\text{x}10^3$ moles/m^3, $C_{eq} = 0.2$ mole/m^3, and $\theta = 0.1$, we find that the rate of weathering front advance is 80 m/Myr. The factor converting recharge rate to weathering front advance rate is therefore indeed small, here of order 10^{-4}.

In the 1D column simulations, a steady erosion rate at the surface (30 m/Myr, as in our 2D simulations) governs a vertical advection speed of rock through the column. We present three simulations (Figure 7). The first two differ only in the rate of recharge: dry case U_0=0.02 m/yr; wet case U_0=0.12 m/yr. The third simulation repeats the wet case simulation, but expands the depth of the model system from 30 m to 90 m. In these 1D models, fresh

rock is introduced into the bottom of the domain at a steady rate fixed by the denudation rate of 30 m/Myr. This contrasts with the 2D models, in which fresh rock is allowed to weather only when it encounters the base of thegroundwater flow system, i.e. once its elevation is greater than that of the base of the channel,z_b.

The resulting profiles demonstrate the profound influence of recharge rate on the pattern of weathering. As in the 2D simulations, dry case weathering is constrained to a thin near-surface zone (Figure 7a), whereas wet case weathering extends through the entire modeled depth (Figure 7b). Note that unlike the figures from our 2D simulations, in which the model domain was fixed and the ground surface lowered through time, in the 1D simulations shown in Figure 7 the model domain moves down with the ground surface. These simulations therefore reveal the temporal variations in thickness of the weathered zone (equivalently, the rock enters the base of the system at a prescribed rate of lowering of the landscape). The weathered zone in the dry case (Figure 7a) exhibits a relatively low reaction extent (i.e., significant fresh plagioclase remains in the weathered zone), and the thickness of the weathered zone does not change significantly over the 1000 kyr model run; a steady weathering boundary layer has evolved at the top of the system. In the wet case (Figure 7b), the weathering front sharpens over time as the region in which plagioclase is almost fully depleted thickens over time. The weathering front finally reaches near the bottom of the moving 30-m model domain depth and then exhibits near steady behavior to the end 1000 kyr model run, shown by successive reaction extent profiles plotting on top of each other. At this point, water traveling downward through the rock encounters essentially no plagioclase until it nears the basal boundary to the water system. A weathering boundary layer evolves at the base of the system. Extending the model depth in the wet case by three-fold (Figure 7c) effectively removes the role of a base to the system, given that we only run the model for 1 million years. In the absence of a base to the hydrologic system, the weathering front

continues to advance downward without producing a steady state. Similar behavior was noted by Lebedeva&Brantley (2010; 2013) in their models of regolith production and hillslope evolution based on assuming one-dimensional vertical flow.

The difference between dry and wet cases is well captured by the ratio of two speeds: weathering front advance rate and exhumation rate: w_f/e, as also noted by Lebedeva& Brantley (2010). The importance of a similar dimensionless parameter was also highlighted by Braun et al. (2016), whose analysis considers only flow and weathering below the water table (although their model appears to relate a vertical weathering front propagation velocity to a horizontal groundwater flow velocity). In all of the cases considered here, the exhumation rate e = 30 m/Myr. In the dry case, the weathering front speed is 13 m/Myr, and the ratio is therefore 0.43, well less than 1. In the wet case, the reaction front speed is 80 m/Myr, and the ratio is therefore 2.7, well more than 1. The final depth of the reaction front in Figure 7c is ~50 m, and corresponds to 80 m of weathering front advance, minus 30 m of exhumation over the 1000 kyr simulation.

The contrast in wet case results shown in Figures 7b and c illustrates the importance of the bottom boundary condition when $w_f/e > 1$. If the base of the system is very deep, as in Figure 7c, the weathering front simply proceeds through the rock in a one-dimensional model and produces neither a steady-state profile nor regolith thickness (similar to Lebedeva& Brantley, 2010). Importantly, however, if the base of the system is encountered at shallower depths, a steady state does develop, with a basal boundary layer of weathering underlying a thick regolith. The 2D results illustrate that in reality the base of the system is dictated by the location of the channels adjacent to a hillslope; these serve as drains for the groundwater, to which lateralgroundwater flow is steered. While a 1D view captures the behavior of the 2D dry case very well, it fails in the wet case, as weathering takes place along flowlines that are diverted hyperbolically toward horizontal flow at the channels that serve as the water drains

for the hillslope. This is especially the case during the transient phase as the landscape is far from topographic and weathering steady state (Figures 3 and 4). Thus, our 2D modeling approach that incorporates both vertical flow in the vadose zone and a horizontal component of flow below the water table produces fundamentally different behavior compared to a 1D model at high recharge rates, demonstrating that a steady-state regolith profile can develop even in these cases due to the influence of lateral groundwater flow toward a channel.

4 Discussion

Our models produce distinctly different patterns of weathering across the hillslope in the dry and wet cases we tested, and we identify a metric for the transition from one behavior to the other. The weathering front in the dry case proceeds vertically (Figure 3a-c, 4a-d), confined to a thin layer near the surface. The dry case behavior is captured adequately by a one-dimensional vertical model (Figure 7a). In contrast, rapid travel times in the wet case propagate active weathering below the water table (Figure 3d-f, 4e-h), and the pattern across the hillslope is not captured by the one-dimensional vertical flow and reactive transport models shown in Figures 7b and 7c. The 2D wet case weathering front becomes pegged at the base of the groundwater system, where horizontal water flow (Figure 2b) focuses weathering reactions in relatively unweathered rock. We have found that the results are insensitive to the length of the hillslope, L; the basic patterns we have presented are unchanged.

Under a steady climate/hydrology and a constant rate of stream incision, steady state topography and critical zone architecture develop in both the wet and dry cases, when viewed in a coordinate system that lowers with the stream. The surface topographies in both cases are identical because we have not included explicit dependence on the degree of weathering in either soil production w, or the soil transport rate Q. In particular, our coupled model of erosion, hydrology and weathering produces a deep flat-floored pattern of highly weathered

material that is therefore deep below the interfluve and shallow adjacent to the channel in the wet case, which contrasts with the relatively thin surface-parallel weathered zone in the dry case. While the floor of the groundwater flowfield is flat with a base at the bottom of the channel in our simple model, the groundwater flow domain may in fact extend below the base of the channel (e.g., Banks et al., 2009; Ameli et al., 2016). More detailed models that account for deep groundwater circulation in the sense of Tóth(1962) should lead to a weathered zone that could become bowed downward below the interfluve. As in both the wet case in our 2D models and the 1D profile in a bounded system (Figure 7b), the pattern should display a weathering boundary layer at the base of the groundwater system, no matter what geometry the base of the system takes on. We note as well that once these more complex numerical solutions to the flowfield are enacted, weathering reactions may occur beneath the channel itself in some cases. This would allow us to explore the degree to which weathering preparation of the rock could influence the rate of channel incision. We will incorporate these realistic features in future simulations.

The depth of the weathering zone reflects the competition between downward weathering front advance controlled by water flow, and the apparent upward motion of the rock relative to the ground surface controlled by the erosion rate. The dramatic differences in the patterns and degree of weathering within the hillscape hillslopes in different landscapes can be captured by the ratio of two rates: the rate of weathering front advance, and the rate of incision, w_f/e. In the dry case, much of the rock remains unweathered, and a thin weathered layer develops parallel to the surface. In the wet case, weathering goes to completion within much of the hillslope, leaving only a thin weathering boundary layer at the base of the system where rock first enters the weathering system from below. This is seen in the 2D simulations (Figures 3 & 4), and itsessence may be captured by imposing a floor to the system through which fresh rock rises in the 1D model (compare Figures 7b and c).

Quantitative interpretation of the 1D results using the ratio of weathering front propagation speed to exhumation rate, w_f/e, transfers broadly to the 2D cases. The 2D dry base case corresponds to $w_f/e = 0.43$, whereas the 2D wet base case corresponds to $w_f/e = 2.7$. In the dry case a weathering boundary layer evolves at the top of the system; in the wet case a weathering boundary layer evolves at the base of the system (Figure 3). At some ratio, presumably near unity, we expect a switch in behavior from surface parallel to deep weathering. Indeed this occurs. In Figure 5a, the transitional case shown corresponds to a ratio $w_f/e = 0.94$, and the transitional cases in Figure 6 correspond to w_f/e ratios of 0.7 to 0.95. In all of these cases in which the weathering rate is slightly less than the exhumation rate, a portion of the interfluve near the crest behaves as a dry case in which the weathering front advance is outpaced by the surface lowering rate, as we expect when $w_f < e$; whereas the outer edge of the hillslope near the channel experiences 2D effects of convergent water flow through the rock mass, promoting a behavior more akin to the wet case. These cases both emphasize the importance of the ratio w_f/e as a discriminator of weathering patterns, and further illustrate the importance of the 2D flowfield.

Our models have shown that in wet cases in which the weathering front advances at a rate that exceeds the channel incision rate, considerable weathering can take place below the water table. This contrasts with assumptions made in past work (e.g., Rempe and Dietrich, 2014), in which mineral weathering reactions were restricted to the vadose zone. While this is appropriate in our dry case simulations, in our wet case the high groundwater flow speeds and the low concentrations of remaining primary minerals in the upper portion of the hillslope assure that mineral weathering reactions can indeed proceed well below the water table.

Our modeling framework involves many simplifications. While the assumption of a steady state climate and hydrology over the 1000-kyr simulations is clearly unrealistic, it allows evaluation of the differing behavior in wet versus dry climates. To retain analytical

simplicity, we have also not incorporated the dynamic influence of weathering-driven changes in porosity and permeability into flow and reactive transport calculations. Rather, our model assumes a constant effective hydraulic conductivity for the entire hillslope. If the hydraulic conductivity decreases with depth as expected during weathering, the behavior obtained in the wetter cases may be modified by the restriction of the saturated groundwater flow paths to shallower depths. However, in the drier cases, as not much weathering occurs in the saturated groundwater flow, the behavior is not expected to be significantly influenced by evolution of the permeability field.One could imagine a model strategy in which the hydraulic conductivity structure would evolve with a growing length scale over which the conductivity declines with depth (effectively moving from one to another case illustrated in Ameli et al., 2016). We have, however, shown in Figures 5b and c an end-member case in which the hydraulic conductivity and the porosity were given high values corresponding to fully weathered conditions. That these simulations showed no fundamental difference from our base case runs implies that a simulation in which the hydraulic conductivity is allowed to evolve is likely to yield similar results. We also note that if the overall system permeability is initially dominated by fractures, as is likely the case in granitic terrain that includes both the Calhoun (wet) and Boulder Creek (dry) CZO sites that inspired these analyses, one should not expect the saturated hydraulic conductivity to evolve greatly over time due to weathering. This is because alteration by weathering occurs primarily in the rock matrix that does not contribute significantly to saturated hydraulic conductivity, and isovolumetric weathering implies that matrix block volumes are preserved and fracture apertures are thus not altered significantly (Pandey and Rajaram, 2016). Taken together, these arguments support the claim that the chief driver of the difference between wet and dry cases is the recharge rate. We acknowledge that there is limited understanding of how unsaturated flow properties are altered by weathering. As evident from the simulation results shown in Figure 5a, the water

content in the vadose zone, which regulates the advective solute velocity and that of the weathering front, does exercise some control on the weathering pattern. If the porosity and water content are significantly altered by weathering in a manner that is not accurately captured by isovolumetric calculations we have employed, the weathering front velocity is expected to evolve with time even under a steady recharge forcing. There are significant additional complexities involved in unsaturated flow through fractured rock, such as film flow on fracture surfaces. Additional sensitivity analyses in future work, and explicit incorporation of evolution of the hydraulic properties of the rock mass as it is weatheredare clearly warranted.

We have also assumed that the weathering reactions are simple, bimolecular reactions between a weathering agent and a primary mineral. Such an approach follows closely that of many other teams (e.g., Ortoleva et al., 1987; Brantley and Lebedeva, 2011; Lebedeva and Brantley, 2010; 2013, and Brantley et al., 2017). However, because these models do not explicitly represent the roles of either dissolved oxygen or carbon-dioxide (carbonic acid) on weathering rates, they cannot address the role of a variable water table, which would result inregulation of weathering rates by wetting-drying cycles. At low water contents, dissolved gas concentrations will typically be sustained by gas transfer and dissolution across air-water interfaces.

The rule we have employed for the lowering of the bedrock interface (eq. 4), often called the soil production rule, is simplistic. It depends exponentially upon the local thickness of the soil, and not on any other environmental variable. While there is debate about the shape of the dependence on soil thickness, we ought to expect the entrainment of rock into the mobile regolith layer to depend as well upon the degree of damage of that rock. Such a feedback is not enacted in the present model as we lack both a metric for this susceptibility to

entrainment as well as a mathematical representation of the processes by which rock is entrained. This is a frontier in geomorphology.

A characteristic of CZ architecture seen in some locations,in which the weathered zone is neither surface-parallel, nor consistently as deep as the bounding channels, is not captured with the models presented here. Such a tapered architecture with deeper weathering near the crest has been documented in the Oregon Coast Range (Anderson et al., 2002), northern California (Salve et al., 2012), and in the Mount Lofty Ranges, south Australia (Banks et al., 2009). Our steady state model results do not producesuch downslope tapering patterns of weathering. In contrast, Lebedeva and Brantley (2013) produce such a pattern that reflects their choice of the geomorphic rule set. Anderson et al. (2002) suggested erosion by periodic landslides plays a role in the downslope thinning of weathering layers, a process not incorporated in our models. Exploration of this case therefore requires extension of the geomorphic rule set to embrace both soil and bedrock mass wasting mechanisms.

Rempe and Dietrich (2014) espouse a model of critical zone development in which weathering does not occur until the rock emerges above the water table. This means that the weathered zone is bounded by the surface above and the groundwater table below, which automatically therefore tapers. Rempe and Dietrich assume that the groundwater in the rock below the water table is saturated with respect to the primary minerals, preventing reactions from occurring there. The rock in their model is therefore assumed to be fresh when it emerges above the water table. Our modeling approach naturally calculates weathering reaction rates in the shallow subsurface, based on a reactive transport equation. In our dry end member case, no weathering occurs below the water table; but in the wet end-member case it does. We believe that one cannot generally assert that weathering does or does not occur below the water table. It should depend on the reaction kinetics and recharge rate.

These together govern whether the water is saturated with respect to the minerals present ($C<Ceq$ in equation 12) at any place and at any time in the flowfield.

We argue that subsurface critical zone architectures that our models produce appear to mimic those deduced from the seismic velocity structure at the Calhoun CZO and Boulder Creek CZO sites, in wet and dry climates, respectively (St. Clair et al., 2015). It has been suggested that the dramatic differences between the deeply weathered interfluves in South Carolina (Calhoun CZO) and Maryland, and the shallow surface-parallel interfaces in Colorado (Gordon Gulch in Boulder Creek CZO) can be attributed to the regional far-field stress (St. Claire et al., 2015; Moon et al., 2017). In this conceptual model, far-field compressive stresses oriented normal to ridgelines, as in the South Carolina site, open fractures that promote deep weathering within the interfluve, leading to a "bowtie" pattern in which the interface between fresh rock and weathered rock is deep and is shaped like a subdued mirror image of the surface topography. The authors argue that at the site in Colorado, where far-field compressive stresses are absent, fractures do not open, and the fresh rock interface remains essentially surface-parallel.

Our results present an alternative to this conceptual model in which the differences in weathering patterns are attributable to climate rather than tectonic stress. There are, however, undoubtedly feedbacks between farfield stress, landscape curvature and fracturing of the rock (St. Claire et al., 2016; Moon et al., 2017). These feedbacks would allow the porosity, water retention curve, relative permeability and water content in the vadose zone to evolve, as well as the saturated hydraulic conductivity below the water table. The influences of the degree of weathering of the bedrock on soil production, thereby modifying equation 4, and of the clay content on the soil transport rate, modifying equation 5, should also be included. Only when these feedbacks have been incorporated can we fully explore how the degree of weathering influences the topographic shape of the landscape, and how the two co-evolve. Our hope in

this work has been to establish the basic backdrop against which such future efforts can be compared.

Finally, it must be acknowledged that history matters in the evolution of a landscape and itsweathering. It is not only the present state of stress in a landscape that matters, but the history of stress to which a rock mass has been subjected, that governs the density and orientation of the fracture networks through which reactive water travels (e.g., Molnar et al., 2007). And given the pace at which a landscape evolves, with time scales of order million years to replace the rock volume in an interfluve, the hillslopes will have been exposed to many cycles of climate that ought to pace not only the rate of water delivery to the subsurface, but will modulate the reaction rates involved intheevolution of the weathering profile.This long-term geologic and climatic setting also governs the incision history of the bounding channels that will inevitably differ from one landscape to another. Together these historical effects make it difficult to isolate the role of climate in establishing the pattern of weathering in any particular landscape. We may nonetheless conclude that all else being equal, the pattern of weathering in a landscape will sensitively reflect the water recharge rate to the landscape.

5 Conclusions

Notwithstanding the simplifications noted above, our coupled model of erosion, hydrology, reactive transport and weathering incorporates the dominant processes controlling the co-evolution of an interfluve and the critical zone within it. The difference between the critical zone architectures obtained for two end-member cases that differ only in the imposed recharge mimics that documented in the seismic velocity fields believed to be a proxy for degree of weathering (St. Clair et al., 2015). The pattern depends sensitively on the ratio of weathering front advance to erosion rate. While our modeling results suggest that differences in climate/hydrology alone can yield dramatically different weathering fields, the frontier lies

in incorporation of feedbacks that allow the permeability field to evolve as both weathering and stress-related fracturing proceed.

Acknowledgments

Models are available from the authors upon request and will be archived at CSDMS, CU-Boulder. Funding for this research was provided by the NSF (EAR-1331828) to support the Boulder Creek CZO. We appreciate discussions with CZ scientists at the 2017 national meeting in Arlington, Virginia. We also acknowledge critical and constructive reviews of a previous version of the manuscript by Jennifer Druhan and an anonymous reviewer, and of this version by two anonymous reviewers.

Supporting Information

We present in Supporting Information available online an extended discussion of geomorphic transport rules, and five movies of simulations, two supporting the 2D model runs and three supporting the 1D runs.

References

Ameli, A. A., McDonnell,J. J., & Bishop, K. (2016). The exponential decline in saturated hydraulic conductivity with depth: a novel method for exploring its effect on water flow paths and transit time distribution. *Hydrologic Processes*.doi: 10.1002/hyp.10777

Anderson, R. S. (2002). Modeling of tor-dotted crests, bedrock edges and parabolic profiles of the high alpine surfaces of the Wind River Range, Wyoming. *Geomorphology*, 46, 35-58.

Anderson, R. S., Anderson, S. P., & Tucker, G. E. (2013). Rock damage and regolith transport by frost: an example of climate modulation of the geomorphology of the critical zone. *Earth Surface Processes and Landforms*, 38, 299–316.

Anderson, S. P., Dietrich, W. E. &Brimhall, G. H. Jr. (2002). Weathering profiles, mass-balance analysis, and rates of solute loss: Linkages between weathering and erosion in a small, steep catchment. *Geological Society of America Bulletin*, 114, 1143–1158.

Anderson, S. P., F. von Blanckenburg, & A. F. White (2007).Physical and chemical controls on the Critical Zone.*Elements*, 3, 315–319.

Banks, E. W., Simmons, C. T., Love, A. J., Cranswick, R., Werner, A. D., Bestland, E. A., Wood, M., & Wilson, T. (2009). Fractured bedrock and saprolite hydrogeologic controls on groundwater/surface-water interaction: a conceptual model (Australia). *Hydrogeology Journal* 17, 1969-1989, doi: 10.1007/s10040-009-0490-7.

Befus, K. M., Sheehan, A. F., Leopold, M., Anderson, S. P., & Anderson, R. S. (2011).Seismic constraints on critical zone architecture, Boulder Creek Watershed, Front Range, Colorado.*Vadose Zone Journal*, 10, 915–927.

Brantley, S. L., &Lebedeva, M. I. (2011). Learning to read the chemistry of regolith to understand the Critical Zone. *Annual Review of Earth and Planetary Sciences*, 39, 387–416.

Brantley, S. L., Lebedeva, M. I., Balashov, V. N., Singha, K., Sullivan, P. L., &Stinchcomb, G. (2017). Toward a conceptual model relating chemical reaction fronts to water flow paths in hills. *Geomorphology*, 277, 100–117.

Brantley, S. L. & White, A. F. (2009). Approaches to modeling weathered regolith.*Reviews in Mineralogy and Geochemistry*, 70, 435-484.doi:10.2138/rmg.2009.70.10.

Braun J., Mercier, J., Guillocheau, F., & Robin, C. (2016).A simple model for regolith formation by chemical weathering.*Journal of Geophysical Research: Earth Surface*, 1–81. doi:10.1002/2016JF003914.

Brooks, R. H., & Corey, A. T. (1964). Hydraulic Properties of Porous Media, *Hydrol. Pap.3*, Civil Engineering Department, Colorado State University, Fort Collins, Colorado, 27 pp.

Buss, H. L., Brantley, S. L., Scatena, F. N., Bazilievskaya, E. A., Blum, A., Schulz, M., Jiménez, R., White, A. F., Rother, G., & Cole, D. (2013). Probing the deep critical zone beneath the Luquillo Experimental Forest, Puerto Rico. *Earth Surf. Process. and Landforms*, 38 (10), 1170-1186. doi:10.1002/esp.3409.

Carman, P. C. (1939). Permeability of sands soils and clays. *J. Agric. Sci*., 29, 262–273.

Chesnaux, R., Molson, J. W., &Chapuis, R. P. (2005), An analytic solution for ground water transit time through unconfined aquifers. *Groundwater*, 43(4), 511-517.

Clarke, B. A., & Burbank, D. W. (2011). Quantifying bedrock-fracture patterns within the shallow subsurface: Implications for rock mass strength, bedrock landslides, and erodibility. *Journal of Geophysical Research* 116, F04009.doi:10.1029/2011JF001987.

Crane, M. J., & Blunt, M. J. (1999). Streamline-based simulation of solute transport. *Water Resour. Res.*, 35(10), 3061–3078. doi:10.1029/1999WR900145.

Dagan, G., &Cvetkovic, V. (1996).Reactive transport and immiscible flow in geological media, I, General theory.*Proc. R. Soc. London, Ser. A*, 452, 285-301.

Dixon, J. L., Heimsath, A. M., &Amundson, R. (2009). The critical role of climate and saprolite weathering in landscape evolution.*Earth Surface Processes and Landforms*, 34(11), 1507-1521.

Döll, P. &Fiedler, K. (2008). Global-scale modeling of groundwater recharge,*Hydrol. Earth Syst. Sci*., 12, 863–885.

Freeze, A. R., & Cherry, J. A. (1979). *Groundwater*. Englewood Cliffs, NJ: Prentice-Hall.

Gallen, S. F., Clark, M. K., &Godt, J. W. (2015). Coseismic landslides reveal near-surface rock strength in a high-relief, tectonically active setting. *Geology*, 43(1), 11-14.

Gelhar, L. W.,& Collins (1971).General analysis of longitudinal dispersion in nonuniform flow. *Water Resour. Res*., 7(6), 1511–1521. doi:10.1029/WR007i006p01511.

Gelhar, L. W., & Wilson, J. L. (1974). Ground-water quality modeling.*Ground Water*, 12(6),

399–408.

Gilbert, G. K. (1909). The convexity of hilltops.*Journal of Geology*, 17, 344–350.

Heimsath, A. M., Dietrich, W. E., Nishiizumi, K., &Finkel, R. C. (1997).The soil production function and landscape equilibrium.*Nature*, 388, 358–361.

Hilley, G. E., Chamberlain, C. P., Moon, S., Porder, S., & Willet, S. D. (2010). Competition between erosion and reaction kinetics in controlling silicate-weathering rates.*Earth Planet. Sci. Lett.*, 293, 191–199

Hinch, E. J., & Bhatt, B. S. (1990). Stability of an acid front moving through porous rock.*J. Fluid Mech*., 212, 279–288. doi:10.1017/S0022112090001963.

Holbrook, S. W., Riebe, C. S., Elwaseif, M., Hayes, J. L., Basler-Reeder, K., Harry, D. L. Malazian, A., Dosseto, A., Hartsough, P. C., &Hopmans, J. W. (2014). Geophysical constraints on deep weathering and water storage potential in the Southern Sierra Critical Zone Observatory.*Earth Surface Processes Landforms*, 39, 366–380.doi: 10.1002/esp.3502.

Johnstone, S. A., &Hilley, G. E. (2015). Lithologic control on the form of soil-mantled hillslopes.*Geology*, 43, 83–86.

Katsura, S., Kosugi, K., Yamamoto, N., &Mizuyama, T. (2006).Saturated and unsaturated hydraulic conductivities and water retention characteristics of weathered granitic bedrock.*Vadose Zone Journal*, 5, 35-47.

Lebedeva, M., R. Fletcher, V. Balashov, and S. Brantley (2007).A reactive diffusion model describing transformation of bedrock to saprolite, *Chem. Geol.*, 244(3), 624–645.

Lebedeva, M. I., & Brantley, S. L. (2013). Exploring geochemical controls on weathering and erosion of convex hillslopes: beyond the empirical regolith production function. *Earth Surface Processes and Landforms*, 38, 1793–1807.

Lebedeva, M. I., Fletcher, R. C. & Brantley, S. L. (2010). A mathematical model for steady-state regolith production at constant erosion rate.*Earth Surface Processes and Landforms*, 35, 508–524.

Leopold, M., Völkel, J., Huber, J., &Dethier, D. (2013).Subsurface architecture of the Boulder Creek Critical Zone Observatory from electrical resistivity tomography.*Earth Surface Processes and Landforms*, 38, 1417-1431. doi:10.1002/esp.3420.

Maher, K., Steefel, C.I., White, A.F., &Stonestrom, D.A. (2009). The role of reaction affinity and secondary minerals in regulating chemical weathering rates at the Santa Cruz soil chronosequence. California. *GeochimicaetCosmochimicaActa*, 73, 2804-2831. doi: 10.1016/j.gca.2009.01.030.

Maher, K. (2010). The dependence of chemical weathering rates on fluid residence time.*Earth and Planetary Science Letters*, 294, 101–110.

Molnar, P. H., Anderson, R. S., & and Anderson, S. P. (2007). Tectonics, fracturing of rock, and erosion.*Journal of Geophysical Research*, 112, F03014, doi:10.1029/ 2005JF000433.

Moon, S., Perron, J.T., Martel, S.J., Holbrook, W.S., & St Clair, J. (2017). A model of three-dimensional topographic stresses with implications for bedrock fractures, surface processes, and landscape evolution. *Journal of Geophysical Research: Earth Surface*, 122 (4), 823-846.

Ortoleva, P., Enrique, M. Moore, C., &Chadam J. (1987). Geochemical self-organization I; reaction-transport feedbacks and modeling approach. *Am. J. Sci.*, 287, 979–1007. doi:10.2475/ajs.287.10.979.

Pandey, S., &Rajaram, H. (2016). Modeling the influence of preferential flow on the spatial variability and time-dependence of mineral weathering rates. *Water Resour. Res*., 52.doi:10.1002/2016WR019026.

Parsekian, A. D., Singha, K., Minsley, B. J., Holbrook, W. S., & Slater, L. (2015). Multiscale geophysical imaging of the critical zone.*Rev. Geophys*., 53, 1-26. doi:10.1002/2014RG000465.

Rajaram, H., &Arshadi, M. (2016). A similarity solution for reaction front propagation in a fracture–matrix system, *Phil. Trans. R. Soc.A*,374, 20150424.doi:10.1098/rsta.2015.0424.

Rempe, D. M., & Dietrich, W. E. (2014). A bottom-up control on fresh-bedrock topography under landscapes.*Proceedings of the National Academy of Sciences*, 111, 6576–6581.

Rempe, D. M., & Dietrich, W. E. (2018). Direct observations of rock moisture, a hidden component of the hydrologic cycle.*Proceedings of the National Academy of Sciences*, doi: 10.1073/pnas.1800141115.

Riebe, C. S., Hahm, W. J., & Brantley, S. L. (2016). Controls on deep critical zone architecture: a historical review and four testable hypotheses. *Earth Surf. Process. Landforms*. doi: 10.1002/esp.4052.

Roering, J. J., Kirchner, J. W., & Dietrich, W. E. (1999). Evidence for nonlinear, diffusive sediment transport on hillslopes and implications for landscape morphology.*Water Resour. Res.*, 35, 853–870.

Salve, R., Rempe, D. M., & Dietrich, W. E. (2012). Rain, rock moisture dynamics, and the rapid response of perched groundwater in weathered, fractured argillite underlying a steep hillslope, *Water Resour. Res*., 48, W11528, doi:1 0.1029/2012WR012583.

Simmons, C. S., Ginn, T. R., & Wood, B. D. (1995). Stochastic-convective transport with nonlinear reaction: Mathematical framework. *Water Resour. Res*., 31(11), 2675–2688. doi:10.1029/95WR02178.

St. Clair, J., Moon, S., Holbrook, W. S., Perron, J. T., Riebe, C. S., Martel, S. J., Carr, B., Harman, C., Singha, K., & Richter D. d. (2015). Geophysical imaging reveals

topographic stress control of bedrock weathering. *Science*, 350(6260), 534-538.doi:10.1126/science.aab2210.

Strack, O. D. L. (1984). Three-dimensional streamlines in Dupuit-Forchheimer models.*Water Resources Research*, 20(7), 812-822.

Tóth, J. (1962). A theory of groundwater motion in small drainage basins in central Alberta, Canada.*J. Geophys. Res*., 67(11), 4375–4388. doi:10.1029/JZ067i011p04375.

Von Voigtlander, J., Clark, M. K., Zekkos, D., Greenwood, W. W., Anderson, S. P., Anderson, R. S., &Godt, J. W. (2018). Strong variation in weathering of layered rock maintains hillslope-scale strength under high precipitation, *Earth Surface Processes and Landforms, 43, 1183-1194,* doi: 10.1002/esp.4290.

White, A. F. (2002). Determining mineral weathering rates based on solid and solute weathering gradients and velocities: application to biotite weathering in saprolites. *Chemical Geology*, 190, 69-89.

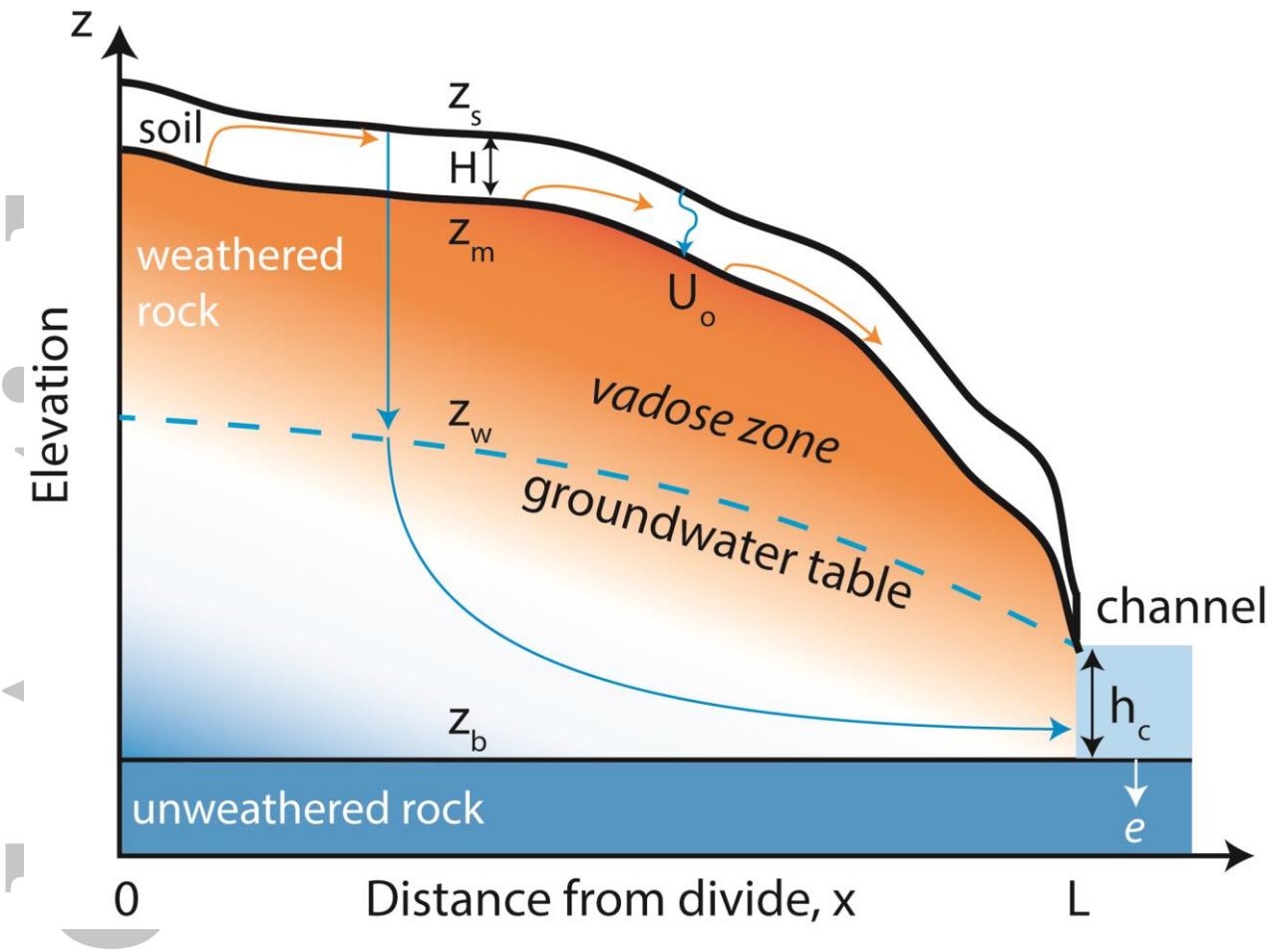

FIGURE 1 Schematic of hillslope model, with elevations of ground surface, z_s, mobile regolith-bedrock interface, z_m, water table, z_w, and unweathered rock, z_b, noted. Infiltration rate, U_o, and hydraulic conductivity, K, govern the water table (blue dashed curve). Water flowpaths (blue arrows) and travel times through the hydrologic system will control the pattern of mineral weathering in the rock. Rock particles transformed into soil (thickness H) travel downslope (brown arrows) toward the channel. The channel (with water depth h_c) serves as the drain for groundwater, and incises into rock at a rate e. As the bottom of the channel governs the base of the water flow system within the hillslope, the rate of channel lowering paces the delivery of fresh rock into the weathering system from the base, z_b, at the rate e. At steady state, the lowering rate of all interfaces is equal to the incision rate of the channel.

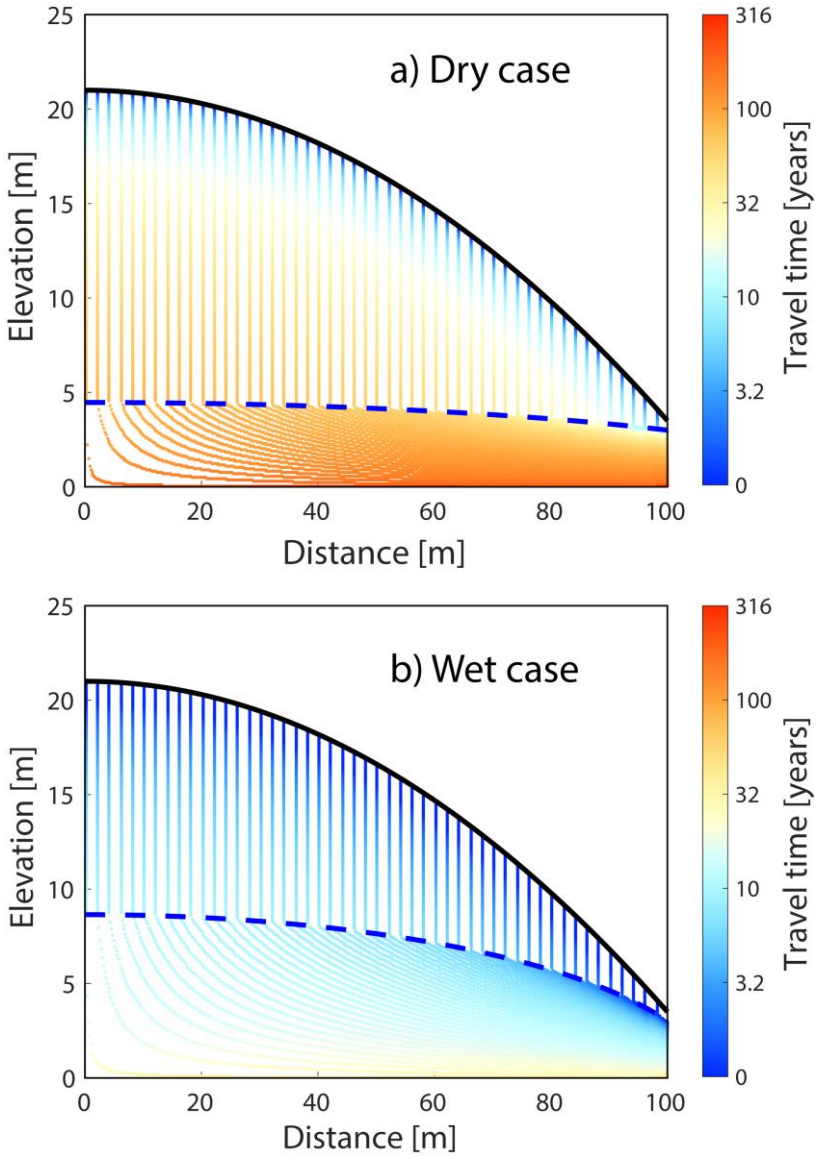

FIGURE 2 Water parcel trajectories and travel times within the interfluve. **a)** Dry case, recharge rate = 0.02 m/yr. **b)** Wet case, recharge rate = 0.12 m/yr. All other parameters are the same. Hydraulic conductivity is uniform at K = 0.05 m/d. The surface topography (black line) is a steady state parabolic form expected for channel lowering rate of 30 m/Myr, and soil diffusivity of $\kappa = k/\rho_s$ = 0.01 m^2/yr; the topography has the same shape and relief as the final forms in Figure 3. Dashed blue line depicts water table.

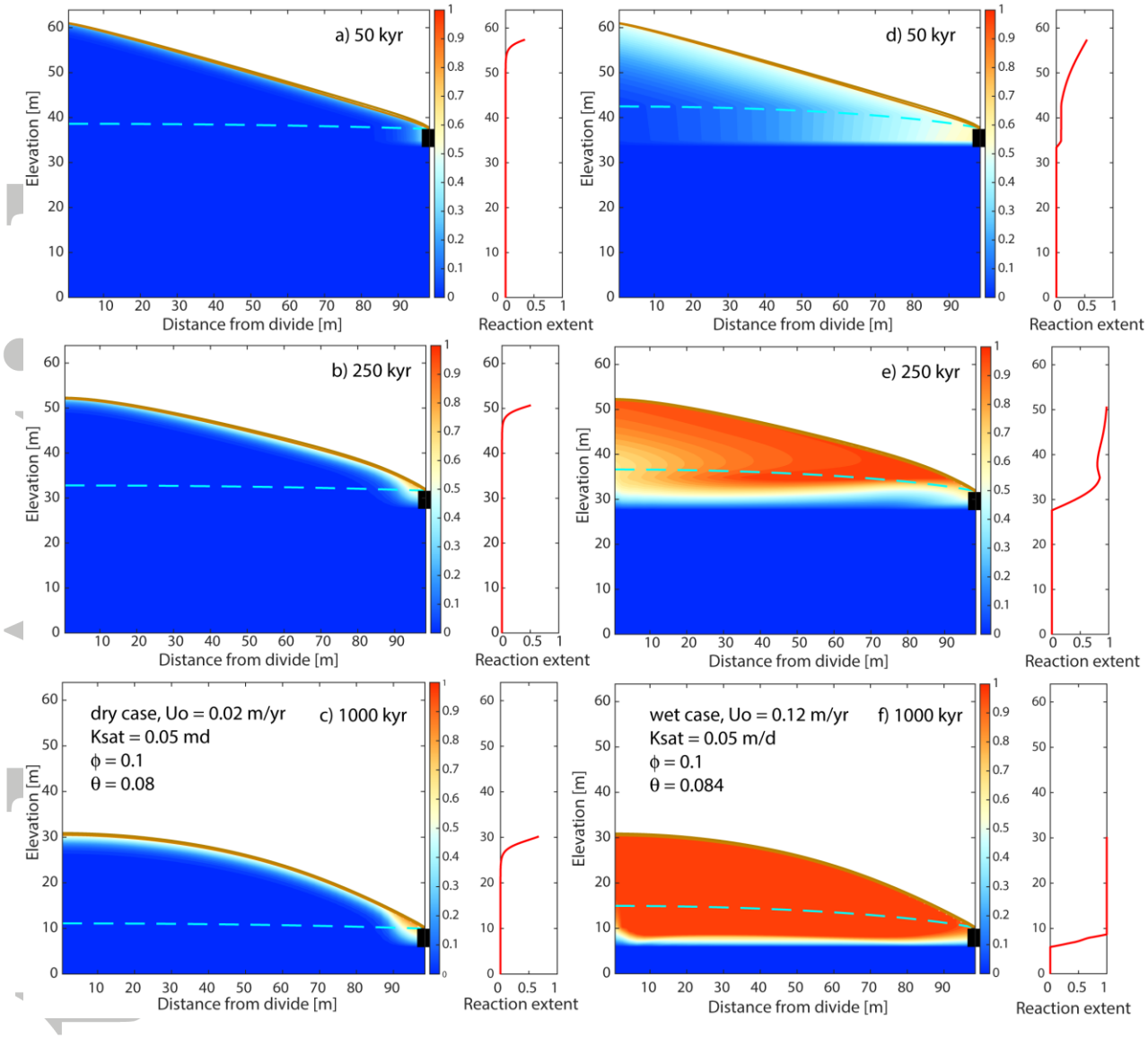

FIGURE 3 Snapshots at 50, 250 and 1000 kyr of reaction extent, 1-(P/P_0), across the landscape (left two frames) and of a 1D vertical profile of plagioclase-kaolinite reaction extent taken at x = 20 m in the landscape (extreme right). Colors correspond to reaction extent [0 1] shown in colorbar. **a-c**) dry case; **d-f**) wet case.In all, initial topography is straight with slope of 0.25, and becomes parabolic. Water table (dashed blue curve) lowers with the bounding channel (black bar at right) at a rate of 30 m/Myr. Animations of dry case and wet case are available in Supporting Information as movies MS1 and MS2, respectively.

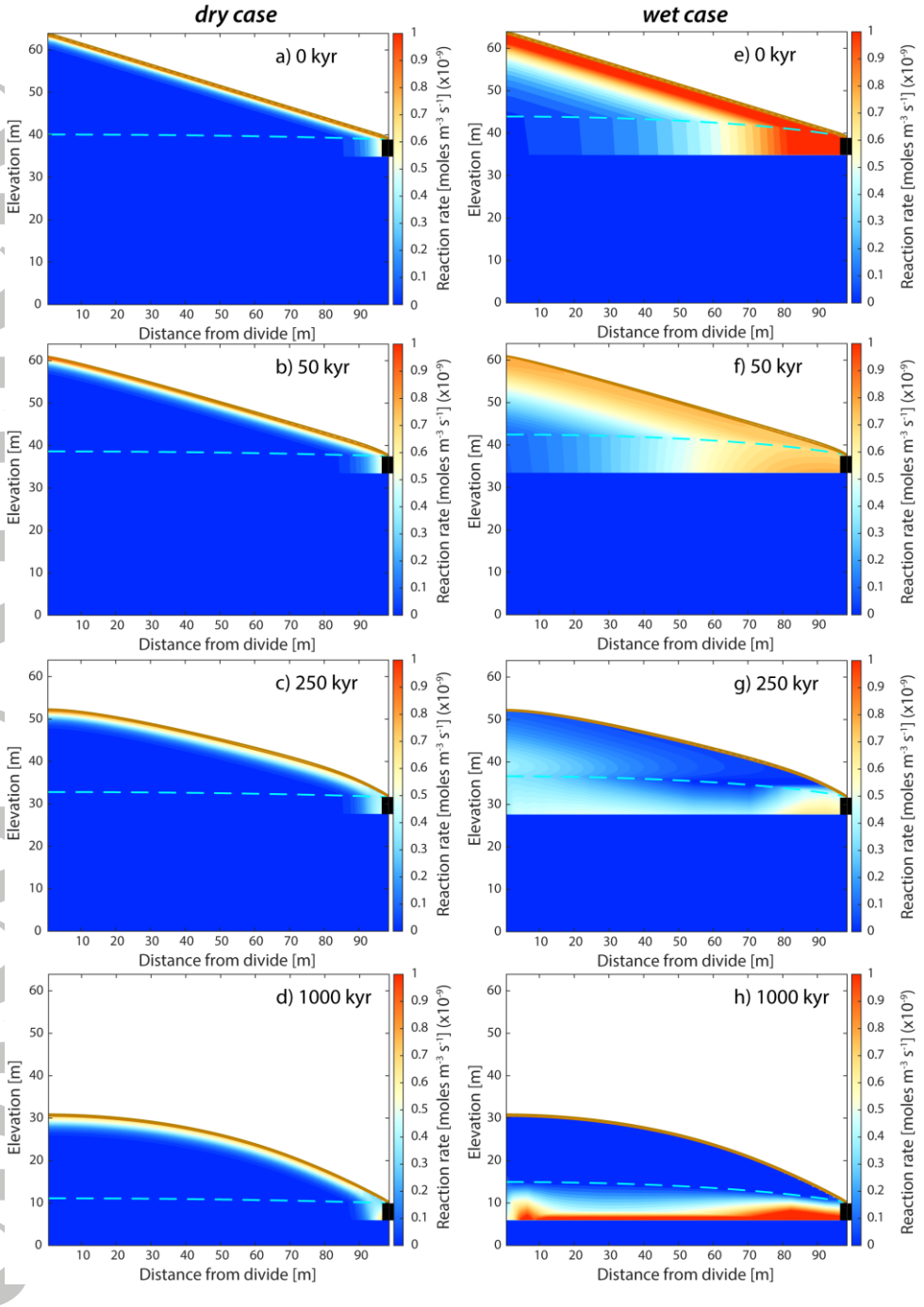

FIGURE 4 Weathering rate fields at 0, 50, 250 and 1000 kyr for same runs shown in Figure 3: **a-d**) dry case; **e-h**) wet case.

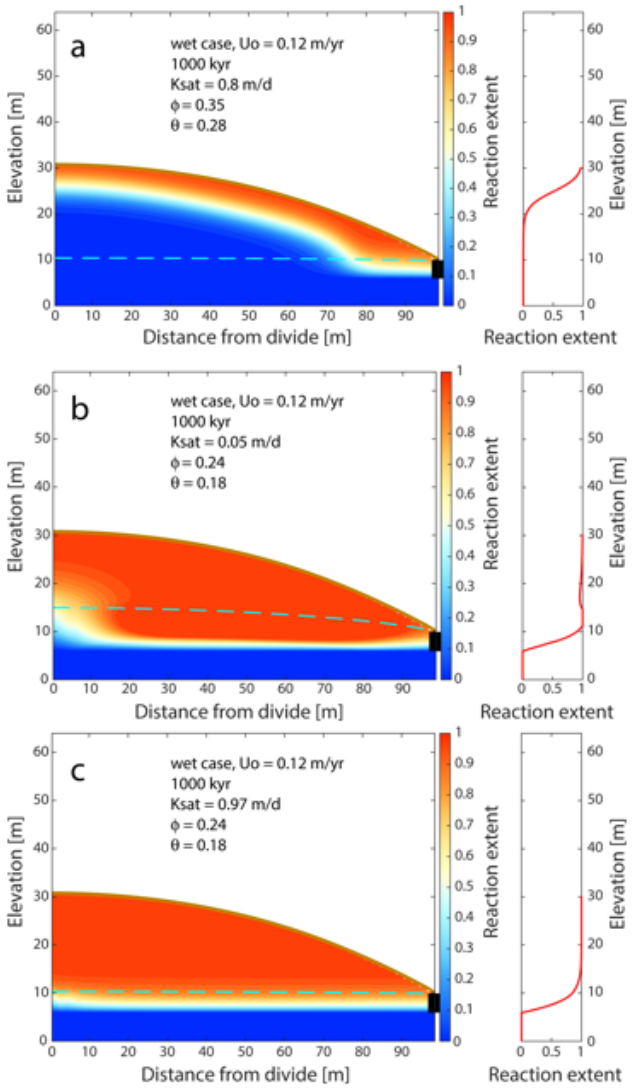

FIGURE 5 Sensitivity of 1000 kyr wet case simulations to choice of hydraulic properties, to be compared with base wet case in Figure 3f with small porosity, water content and saturated hydraulic conductivity corresponding to fractured granite. a) Parameters suggested by a high porosity end-member discussed in Katsura et al. (2006): K_{sat} = 0.8 m/d, porosity ϕ=0.35, and water content θ= 0.28. b) Same K_{sat} = 0.05 m/d as in base case (Fig. 3f) but using ϕ_{new} and θ_{new} described in text. c) Same as (b) but using $K_{sat,\ new}$ ϕ_{new} and θ_{new}. Right panels: 1D vertical profiles of reaction extent [1-(P/P_o)] in each case, taken at a location 20 m from drainage divide.

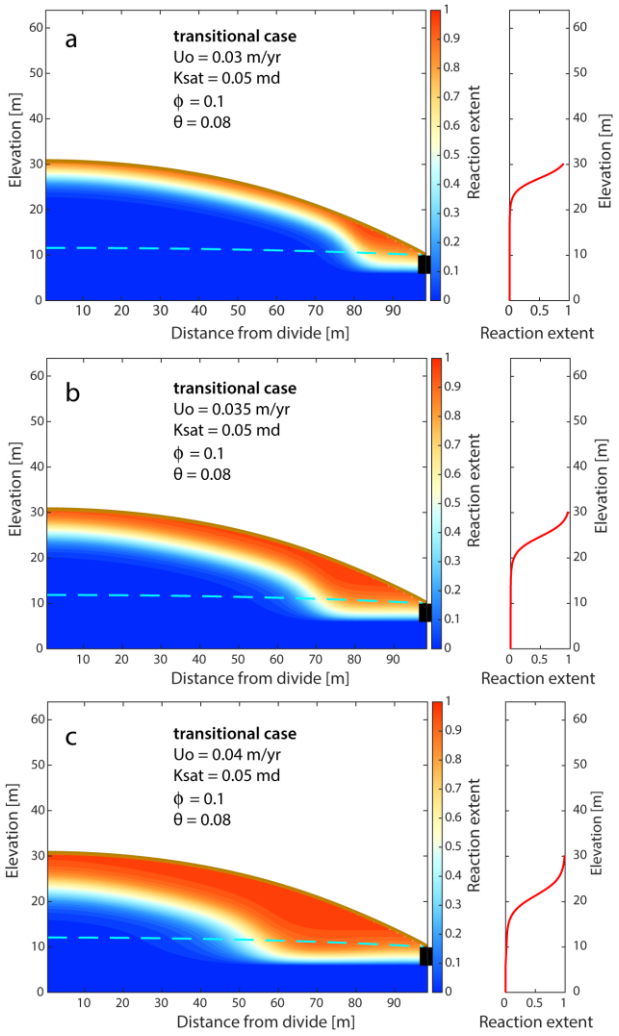

FIGURE 6 Transitional cases with water recharge rates U_0 of a) 0.03 m/yr, b) 0.035 m/yr, and c) 0.04 m/yr. Hydraulic parameters same as base case in Figure 3. Right panel: 1D vertical profile of reaction extent, taken at 20 m from drainage divide. These cases demonstrate that the transitional behavior between the dry case (0.02 m/yr) and wet case (0.12 m/yr) end-members occurs over a narrow range of recharge rates.

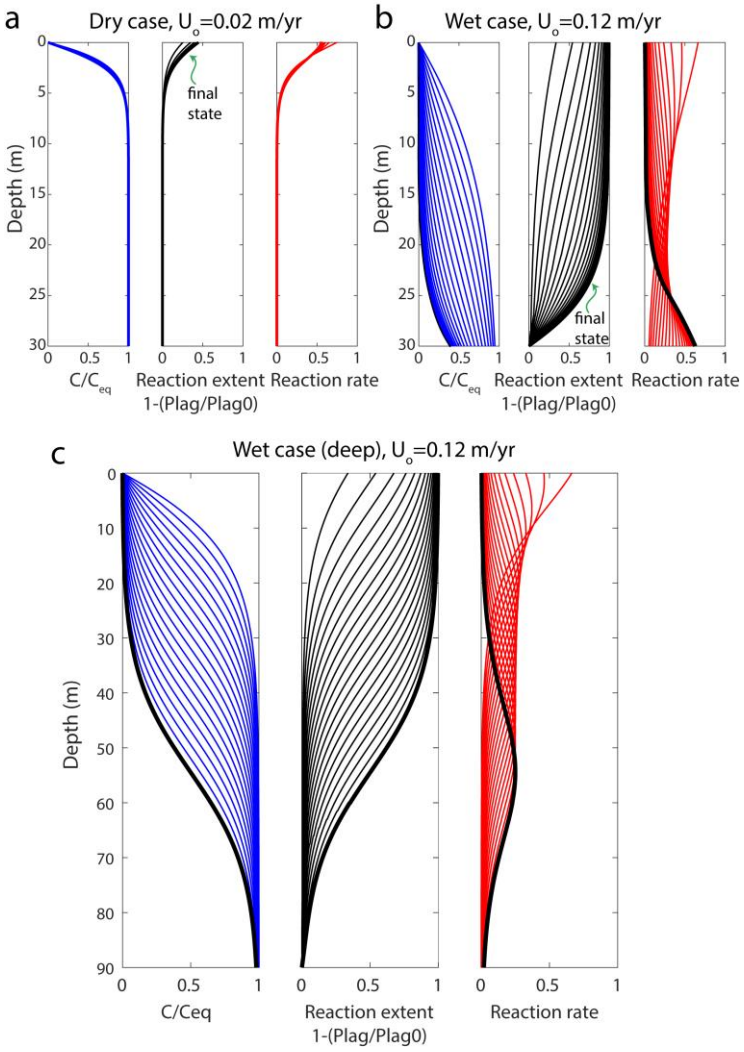

FIGURE 7 1D models of weathering in a) dry case, 30 m model domain, b) wet case, 30 m model domain, and c) wet case, 90 m model domain. In each panel, twenty profiles are shown, recording at 50 kyr intervals over the 1000 kyr run, with the final 1000 kyr profile shown in black. Left columns show the evolution of concentration of weathering products in the fluid (C), normalized by the equilibrium concentration (C_{eq}). Middle columns show reaction extent, 0 being fresh rock, and 1 being complete alteration of plagioclase. Right columns illustrate the instantaneous reaction rate. All cases employ a fixed $\theta = 0.1$. See Movies MS3, MS4 and MS5 in Supporting Information for animations of a), b) and c), respectively.